Single-cell imaging of the lytic phage life cycle dissects the timing and noise in individual infection steps

Charlie Wedd[1], Temur Yunusov[2], Aaron Smith[2], Ruizhe Li[1], Georgeos Hardo[1], Michael Hunter[2], Racha Majed[2], Diana Fusco[2]*, Somenath Bakshi[1]*

[1]Department of Engineering, University of Cambridge, Trumpington Street, Cambridge, CB2 1PZ, UK.
[2]Department of Physics, University of Cambridge, JJ Thomson Avenue, Cambridge, CB3 0HE, UK.

*Corresponding author(s). E-mail(s): df390@cam.ac.uk; sb2330@cam.ac.uk

Abstract

When a lytic bacteriophage infects a cell, it hijacks the cell's resources to replicate itself, ultimately causing cell lysis and the release of new virions. As phages function as obligate parasites, each stage of the infection process depends on the physiological parameters of the host cell. Given the inherent variability of bacterial physiology, we ask how the phage infection dynamic reflects such heterogeneity.

Here, we introduce a pioneering assay for investigating the kinetics of individual infection steps by a single T7 phage on a single bacterium. The high-throughput, time-resolved nature of the assay allows us to monitor the infection progression simultaneously in multiple cells, revealing substantial heterogeneity in each step and correlations between the infection dynamics and the infected cell's properties. Simulations of competing phage populations with distinct lysis time distributions indicate that this heterogeneity can have considerable impact on phage fitness, recognizing variability in infection kinetics as a potential evolutionary driver of phage-bacteria interactions.

Key words:

T7 phage, Single-cell, Microfluidics, High-throughput microscopy, Phage genome injection, Phage infection, Host takeover, Cell lysis

Introduction

Bacteriophages, viruses that infect bacteria, play pivotal roles in shaping bacterial communities in nature and hold significant promise in medicine and biotechnology as biocontrol agents[1,2]. Among them, lytic bacteriophages stand out for their potential in combating antibiotic-resistant infections[2]. As these viruses rely on the host molecular machinery and precursors to proliferate, the infection-to-lysis process intricately depends on the physiological characteristics of the target cell: for instance, factors such as lipopolysaccharide (LPS) composition and receptor density influence the adsorption rate[3]; the resources and machinery of the host cell affect the rate of virion replication[4,5] and the production of lytic agents necessary for cell lysis. Recent single-cell studies have unveiled significant physiological variability among genetically identical bacterial cells, raising questions about how this diversity impacts the kinetics of phage infection and how the variability in infection kinetics, in turn, influences the overall effectiveness of phages in eliminating their target bacteria at a population level[6].

The vast majority of current methods used to study the kinetics of phage infections steps in bacteria rely on bulk culture approaches and omics analysis[7–9], which lack the necessary single-cell resolution to analyse cell-to-cell heterogeneity, or on cryo-EM imaging for high-resolution investigation of structural aspects, which lacks time-resolved information to monitor the progress of individual infection steps and their interrelations[10,11]. In order to quantify and understand how the physiological diversity of host cells influences the infection dynamics of phages, a method is needed that can precisely monitor each stage of infection initiated by a single phage targeting a solitary living bacterium in a time-resolved fashion. Equally important is the need for numerous replicates of these target bacterial cells in a spatiotemporally homogeneous environment to isolate the impact of intrinsic variations in host cell physiology on infection parameters.

Here, we present an innovative approach tailored to address these challenges. Our method harnesses a microfluidic platform engineered to maintain isolated populations of target cells under uniform growth conditions, to enable the tracking of infection dynamics as individual cells become infected and lysed by individual phages. Using high-speed scanning time-resolved microscopy[12], and a combination of fluorescent markers on the model system of phage T7, we are able to follow individual infection events from phage adsorption to cell lysis on individual cells of *Escherichia coli*. Altogether, the method provides the first quantification of the variability in the kinetics of lytic phage infections. Moreover, employing this method allows us to correlate the observed fluctuations in infection parameters with the physiological parameters of the host, thereby elucidating the source of such variations.

Analysis of these comprehensive datasets has yielded unprecedented insights into the temporal dynamics and variability of each infection stage, revealing their interrelationships and broader implications in terms of selective pressure on phage populations. Our results show that the detailed distribution of these kinetic parameters plays a critical role in determining the competitive fitness of a lytic phage, suggesting that variability in the phage life history parameters could constitute an evolutionary trait that is currently unexplored. Looking forward, we anticipate that our method will offer the opportunity to quantify the

distribution of infection parameters, revealing an understanding of phage-bacteria interactions and their evolution previously unattainable.

Results

Single cell imaging of the T7 phage infection cycle

To identify and monitor the timing of the different steps in the T7 life cycle using fluorescence microscopy, we introduced two fluorescent labels in the phage (Fig. 1a). First, we modified the wild-type T7 genome to include a fluorescent reporter of capsid gene expression (gp10A-B, methods). The capsid genes are among the most highly expressed T7 genes[13], making them an excellent target to obtain a strong fluorescent signal for phage transcription. mVenus NB, a yellow fluorescent protein (YFP) with a very fast maturation time (4 min)[14], was selected as suitable fluorescent reporter given the short phage life cycle (15-20 min)[15]. This modified T7 phage was then stained with a DNA binding dye, SYTOX Orange (Fig. 1a, Methods), to visualise phage adsorption to the host cell (t_0) and subsequent genome injection. SYTOX Orange is spectrally compatible with the YFP reporter, has been previously used for labelling lambda phage genome[16] and does not affect cell growth[17].

Individual phage infection cycles in single bacterial cells (*E. coli* MG1655 7740 ΔmotA) were monitored using a modified version of the 'mother machine' microfluidic device[18]. In this device, cells are cultivated in linear colonies within narrow (1.4 μm wide) trenches, receiving nutrients diffusively from the media flowing through the orthogonal flow channel (Fig. 1b). In contrast to the regular mother machine design[19], the narrow trenches are flanked by shallow side trenches that facilitate the diffusion of both nutrients and phage along the length of the trench[18]. We found that the presence of side trenches is essential for phages to infect cells deeper in the trench, so that infection events can be monitored over time all the way to lysis before the corresponding infected cell is pushed out of the trench by the replicating cells above (methods). As individual lineages are isolated in their own trenches and the media continuously flows throughout the experiment, the device maintains cells in a spatiotemporally uniform environment. This uniformity is crucial to minimise potential sources of heterogeneity arising from a non-uniform environment and truly quantify the stochasticity of individual steps in the infection process across a bacterial population experiencing identical external conditions.

The cells are loaded into the device and grown in LB Miller with pluronic for a minimum of three hours to allow them to reach a steady-state exponential growth phase. Subsequently, the growth media is switched to the same media with added phage (methods). High-speed time-resolved scanning microscopy[12] was used to collect multichannel data at high time-resolution (2 frames min^{-1}) during the infection events and processed using a machine-learning model trained with synthetic micrographs[20] (methods), to quantify cell physiology and infection markers over time. Example multichannel image data of a single infection event is shown in Fig. 1c and its corresponding time-series data in Fig. 1d (methods). In the orange channel, the adsorption of the SYTOX Orange stained phage to a cell is seen as an orange dot (t_0), which fades and disappears over time as the genome is

injected (t_1). In the yellow channel, the YFP signal of the capsid production reporter can be seen increasing in intensity (t_3) after genome injection is completed and up to cell lysis. The phase contrast channel shows cell growth up until a point, post-phage-adsorption, when the growth in length stops abruptly (t_2), and the cell eventually lyses (t_5). In the following sections, we analyse the heterogeneity of each of these steps across different infection events.

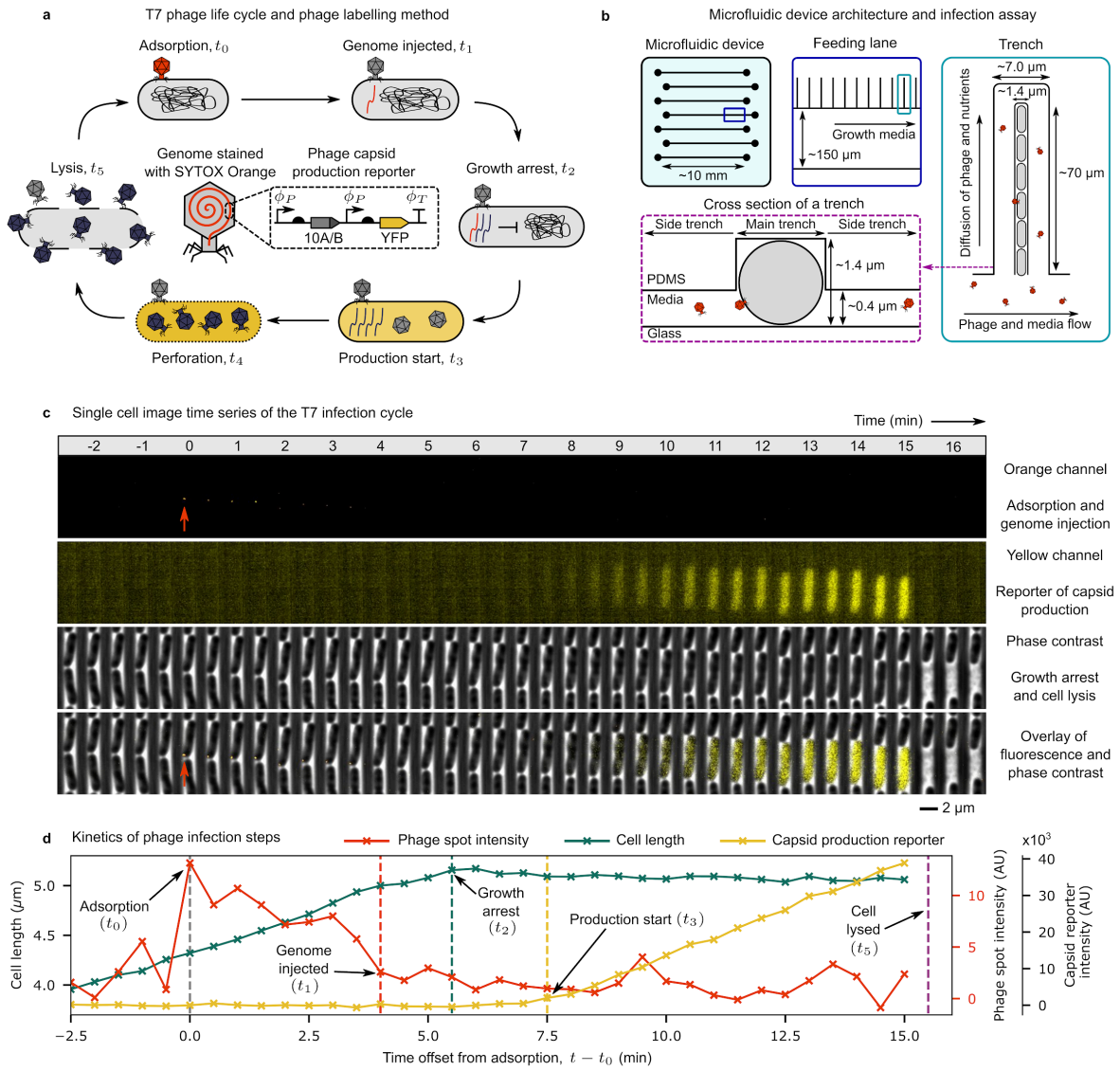

Fig. 1: An assay for imaging the T7 phage infection cycle at the single cell level
a. An overview of six key time points in the T7 life cycle which we use throughout the study to quantify the kinetics of infection steps in the phage life cycle. The DNA staining method and genomic location of the capsid production reporter are indicated in the centre of the loop. **b.** A description of the microfluidic device and infection assay used in this study. **c.** Kymographs showing a T7 phage (indicated by the red arrow) infecting a single bacterial cell. The orange channel image has been bandpass filtered to remove bleedthrough from the YFP capsid production reporter (methods). **d.** Time series data corresponding to the phage infection images presented in (c) demonstrate the typical progression of signals during T7

infection. With the exception of perforation, which happens very close to lysis, all time points from Fig. 1a are labelled on the time series.

Bimodality in genome injection kinetics

The molecular mechanisms that lead to T7 genome entry have been extensively studied[21–24] and result in a three-step process: (i) the first 600 base-pairs enter the cell as the phage tail penetrates the cell wall and membrane, (ii) the host RNA polymerase (RNAP) recognizes a series of binding sites on the genome and translocates it while transcribing the early genes, including the T7 RNAP, (iii) once expressed, the T7 RNAP takes over the process and pulls in the remaining 85% of the genome.

Studies in bulk cultures have shown that the whole process takes approximately 4 minutes on average[25,26], however, the variability of its dynamics within a population is unknown. In our setup, we can track such dynamics across multiple infection events, by quantifying the fluorescence signal coming from the labelled phage DNA over time (Fig. 2, methods). When the phage binds to a cell, a bright spot suddenly appears in the orange channel due to the immobilisation of the phage upon adsorption (Fig. 2c). The fluorescence intensity of the spot then decreases over time as the genome gradually leaves the viral capsid and enters the cell.

Across multiple adsorption events, we observed significant heterogeneity in the progression of genome injection (Fig. 2d-e). The intensity trends reveal two broad classes of entry dynamics. In one, the injection progresses steadily to completion at an approximate rate of 4 kbps min^{-1} (methods). In the other, the entry proceeds similarly up to approximately 1.5 min, but then a sudden transition occurs in which the rest of the genome quickly enters the cell. These results suggest two potential modes of entry. The first class of trajectories would be consistent with the host RNAP being responsible for translocating the whole phage genome into the cell (*E. coli* RNAP's transcription velocity is between 1.2 and 5.4 kbps min^{-1})[27]. The second class aligns with the established three-step genome entry process, in which the first 6 kbps of the phage genome are translocated by the host RNAP and the rest by the much faster T7 RNAP. The distribution of the injection time duration (Fig. 2e) displays a mean duration time of 4.9 min, consistent with previous bulk experiments, but also further reveals the bimodality of the process in which approximately ⅓ of the injection events belong to the first class, and ⅔ to the second.

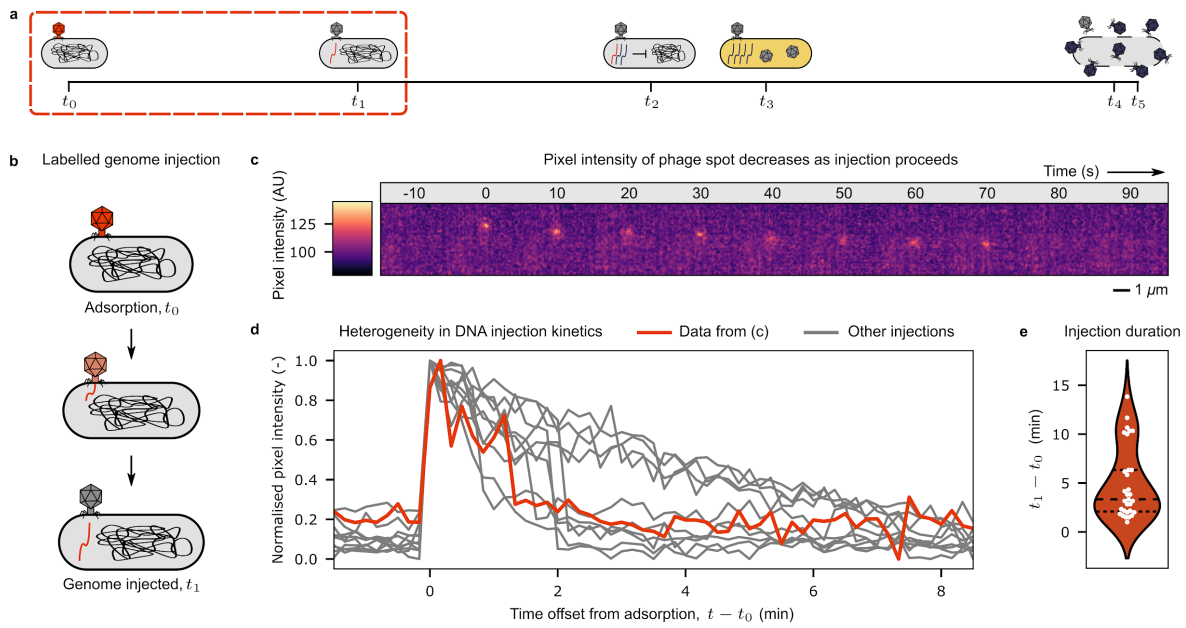

Fig. 2: Heterogeneity in phage genome injection kinetics
a. A timeline showing the temporal location of genome injection in the T7 life cycle. **b.** A schematic of T7 genome injection. **c.** A kymograph of genome injection shown as a heat map. The phage spot moves vertically downwards in sequential frames due to cell growth. **d.** A comparison of phage spot intensities over time for several genome injection events. Signals have been background corrected and normalised. The injection shown in (c) is displayed in orange and examples of ten other injections are displayed in grey. **e.** Violin plot showing the distribution of genome injection durations (t_0 to t_1). The central dashed line represents the median and the outer dashed lines the first and third quartiles. The mean injection duration is 4.9 min (n = 31, CV = 74%).

Host cell shutdown and phage gene expression

The T7 early genes, transcribed very early in the infection process by the host RNAP, are responsible for the shutdown of the host cell, including the inhibition of cell wall synthesis[28,29]. We therefore expect cell growth arrest to be among the first signs that phage proteins are being produced. Our fluorescent transcriptional reporter for the capsid proteins, in addition, pinpoints the onset of expression of late (class III) genes from the phage genome. Together, these two markers allow us to analyse the production dynamics in the infection process and the variability in protein production rate (Fig. 3).

A representative time series data from a single infection event is illustrated in Fig. 3b. The green line depicts cell length, $L(t)$, where the abrupt periodic drops in cell length prior to infection correspond to cell division events. The instantaneous growth rate for each cell is calculated from the local slope of the $\ln(L(t))$ time series (Fig. 3c, Table 6). The precise moment of growth arrest (t_2) is determined when the instantaneous growth rate falls below a given threshold (methods). Soon after growth arrest is detected, we observe the level of capsid expression (YFP signal, yellow line) to increase rapidly until lysis occurs (Fig. 3b). We found that the intensity of capsid expression reporter, $I(t)$, rapidly increases at the start, and that the rate of increase gradually slows down before the infected cell lyses. To compute the

rate of production, α, we use the mean of the instantaneous slopes of the $\ln(I(t))$ time series between 2 and 4 min after the production start time, t_3 (Fig. 3c, Table 6). The exact production start time (t_3) is defined as the first time point after the YFP signal exceeds a given threshold (methods).

Growth arrest dynamics are found to be remarkably robust across different infection events (Fig. 3d). Cells transition from pre-infection growth rates to complete cessation within 3-4 min and in a consistent fashion, independently of their size or position in the cell-cycle. By contrast, expression of the capsid reporter displays considerable variability (Fig. 3d), with the final intensity of the reporter varying by almost an order of magnitude across infection events. In five of the 23 example infections presented in Fig. 3d, the YFP intensity sharply decreases in the final observation before lysis (highlighted in blue, Fig. 3d). This decline in signal coincides with the perforation of the cell envelope in the final moments before lysis, which we will discuss in the next section (Fig. 4). The phenomenon is only observed in a fraction of the infection events due to the short interval between perforation and lysis compared to the frame rate of the images taken (with a mean perforation to lysis time of 6.8 s, as shown below in Fig. 4, we only expect to observe the drop in YFP in 23% of infections when imaging at 2 frames min^{-1}).

Unlike the genome injection process discussed earlier, the time intervals between growth arrest and subsequent lysis (t_2 to t_5) and between start of capsid production and lysis (t_3 to t_5) are narrowly distributed (respectively, coefficient of variation (CV) of 13% and 20%, Fig. 3e), with the latter delayed on average by 1.7 min compared to the first. We note here, that the folding and maturation of the reporter proteins can take minutes, implying that actual expression of the capsid genes might start at the same time, if not earlier than the growth halt of the host cell. Taken together, these results suggest that once the phage has taken control over the cell, the timing of events proceeds almost deterministically.

While the timing of these events shows remarkable robustness, the variability in protein production hints to other sources of stochasticity. Fig. 3f shows the maximum total YFP intensity in each cell versus production rate, α, production time (t_3 to t_5), and the growth arrested cell length, L_{GA}. While we find a positive correlation between production time and maximum YFP intensity, as one would expect, the trend alone is not sufficient to explain the observed variability in protein production. Protein production rates exhibit an even stronger positive correlation with maximum YFP intensity. Interestingly, we find that both production rates and production times typically increase with the length of the growth-arrested cell. Larger production rates in larger cells would be consistent with the presence of more ribosomes, which is likely the limiting factor in phage protein production. The reason behind the positive correlation between production time and cell size is less clear: lysis, which marks the end of production, is thought to be controlled by the accumulation of holins in the cell up to a critical concentration[30,31], thus requiring a larger number of holins in larger cells. However, since larger cells produce proteins exponentially more rapidly, the time to lysis is expected overall to decrease with increasing cell size. The positive correlation between time to lysis and cell length that we observe instead suggests the presence of additional

mechanisms that play a role in controlling lysis, in line with more recent proposals from evolutionary studies[30,32].

While our method currently lacks a direct way to measure burst size, the total expression of YFP at the point of lysis could serve as an indicative measure, as it is designed to be proportional to the number of capsid proteins produced. Our results then suggest that burst size could vary over an order of magnitude across infection events, with this variability being strongly correlated with the size of the growth arrested cell.

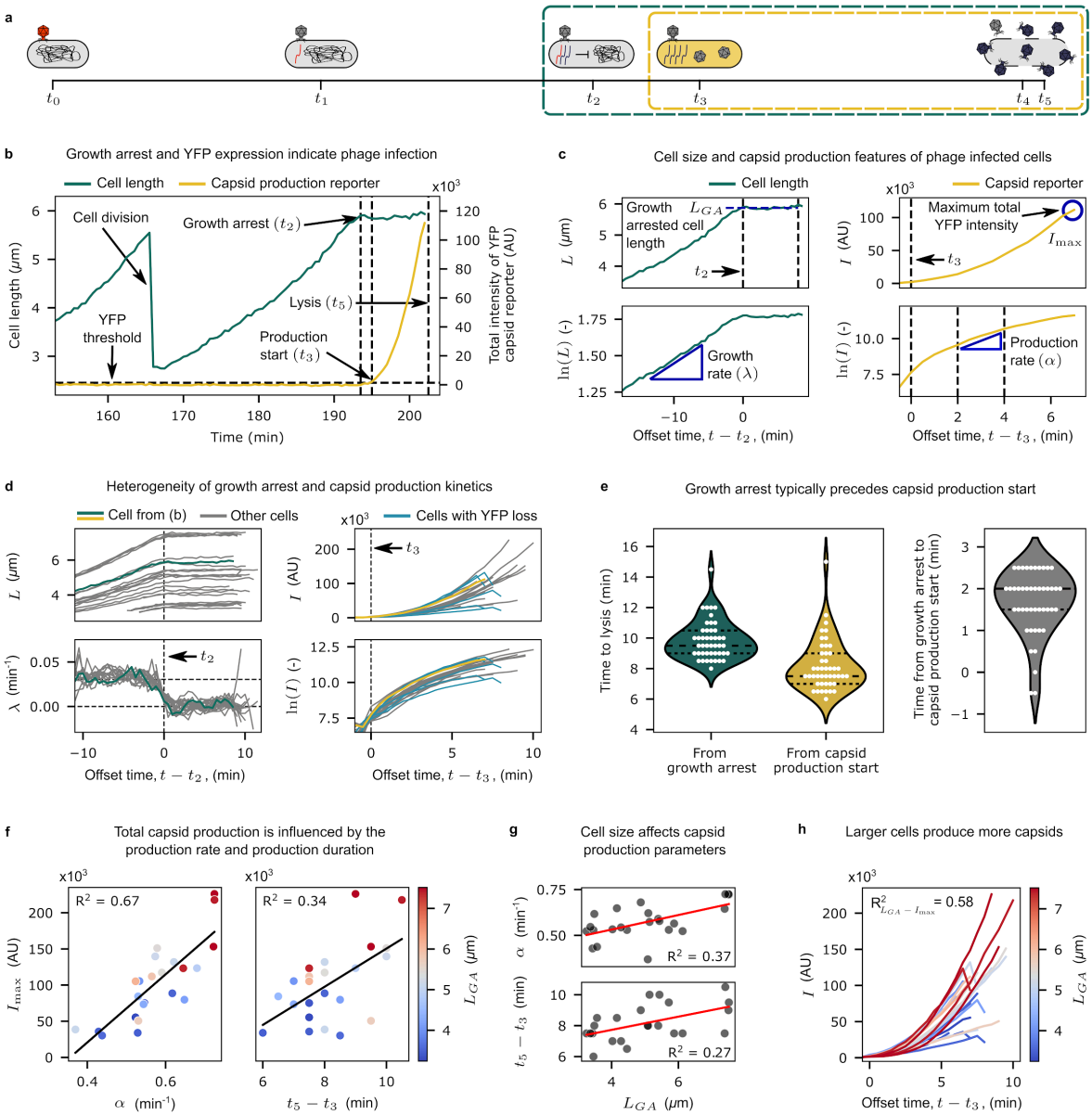

Fig. 3: Kinetics of host shutdown and phage gene expression

a. A timeline showing the temporal location of growth arrest and capsid production start in the T7 life cycle. **b.** Example time series data showing representative cell length and capsid reporter expression data of a cell which becomes infected. Three time points, the growth arrest (t_2), capsid production start (t_3) and lysis (t_5), are indicated. The threshold intensity for production start is also indicated. **c.** An explanation of the quantities used in the analysis of cell growth arrest and capsid reporter production. We use the growth arrested cell length as

a measure of cell size (left, top panel). The cell growth rate is calculated as the instantaneous slope of the natural log-transformed cell length (left, bottom panel). The maximum total YFP intensity, summed over the area of a cell, is a proxy for the total production of capsid proteins (right, top panel). The mean of the instantaneous slopes of the natural log-transformed total YFP intensity between 2 and 4 min after the start of capsid production is used as a measure of the production rate of YFP (right, bottom panel). Detailed descriptions of the calculation of these quantities can be found in Table 6. **d.** Comparison of the cell length (left, top panel) and growth rate (left, bottom panel) between the cell in panel (b) (green lines) and 22 other infected cells (grey lines). The growth arrest kinetic is highly consistent between cells. Comparison of the total YFP intensity (right, top panel) and the natural log-transformed total YFP intensity (right, bottom panel) between the cell in panel (b) (yellow lines) and 22 other infected cells (grey and blue lines). The blue lines highlight the subset of five cells where the YFP intensity sharply drops in the final observation before lysis. The loss of YFP signal is caused by the perforation of the cell envelope just prior to cell lysis (Fig. 4). **e.** Growth arrest typically precedes expression start by a mean time of 1.7 min. The violin plots show kernel density estimates of the timings from growth arrest (green) and expression start (yellow) to lysis, along with the timings of growth arrest to expression start (grey). The central dashed line represents the median and the outer dashed lines the first and third quartiles. The mean time from growth arrest to lysis (t_2 to t_5) is 9.9 min (n = 45, CV = 13%). The mean time from production start to lysis (t_3 to t_5) is 8.2 min (n = 45, CV = 20%). The mean time from growth arrest to production start (t_2 to t_3) is 1.7 min (n = 45, CV = 46%). **f.** The maximum intensity of YFP, our proxy for the total production of capsids in a given cell, is positively correlated with the production rate (left panel, R^2 = 0.67) and the production start to lysis time (right panel, R^2 = 0.34). Markers are coloured by the growth arrested cell length, which demonstrates the tendency of larger cells to produce YFP at a faster rate and to take longer to lyse from the start of capsid production. **g.** The production rate (top panel, R^2 = 0.37) and the production start to lysis time (bottom panel, R^2 = 0.27) plotted as a function of growth arrested cell length. These demonstrate the cell size dependency indicated by the coloured markers in Fig. 3f. **h.** The total YFP intensity in a cell, plotted against the time since the start of capsid production. The lines are coloured by the growth arrested cell length of each cell. This demonstrates that small cells tend to produce fewer capsids, and that larger cells produce more. The maximum YFP intensity as a function of growth arrested cell length demonstrates a positive correlation (R^2 = 0.58).

Cell lysis has two distinct phases

The concluding stage of the infection process involves the lysis of the host cell. As evidenced by the high-resolution data presented above (in Fig. 3d), cells undergo a phase of perforation, characterised by a partial loss of fluorescence signal and phase contrast, before complete lysis ensues. Here, we use high frame rate microscopy to explore the dynamics of cell lysis, recognising that a comprehensive understanding of the final structural alterations occurring during the process may offer insights into underlying mechanisms.

Our initial attempts using 1 frame s^{-1} imaging revealed that the structural changes occurring during lysis unfold on sub-second timescales. Therefore, we used phase contrast imaging at 100 frames s^{-1} to monitor lysis from unlabelled wild type T7 phage on *E. coli* MG1655 7740

Δ*motA* cells. The high frame rate, while conducive to observing rapid dynamics, renders fluorescence imaging unsuitable due to photobleaching and potential phototoxicity. Nonetheless, phase-contrast imaging is sufficient to gain a detailed insight into the material loss from the cell to its surroundings in the fleeting moments preceding lysis (Fig. 4).

The process of lysis unfolds in two distinct phases. The initial phase, termed perforation, is characterised by gradual changes occurring on slower (~1 s) timescales. Perforation involves a gradual leakage of material from the cell, resulting in a subtle increase in phase brightness (Fig. 4b), accompanied by a gradual decrease in the intensity of the surrounding environment. Typically, this phase begins with a small but sharp increase in phase brightness (Fig. 4d), marking the onset of perforation (t_4). Material is then steadily lost from the cell until the commencement of the second phase.

The subsequent phase, referred to as lysis, represents the final structural breakdown of the cell envelope. Occurring at faster timescales of ~0.01 s, this phase is characterised by explosive ejections of material from the cell, culminating in a complete breakdown of the cell envelope (Fig. 4f). Here, the moment when the rate of material loss from the cell experiences the sharpest increase is identified as the onset of lysis (t_{4a}), which ceases when the rate of loss reaches its maximum at the conclusion of lysis (t_5).

The variability in the duration of these events across different infection instances is illustrated in Figs. 4e and 4i. The mean duration from perforation to the onset of lysis is 6.57 s. In contrast, the second phase, spanning from the onset to the end of lysis, occurs much more rapidly, with a mean duration of 170 ms. Our findings demonstrate that the cell envelope is gradually compromised several seconds prior to the final lysis, followed by a swift and complete expulsion of cell debris and phage into the surrounding environment. It is tempting to speculate that the initial perforation marks the action of the holins and other lysis proteins that gradually digest the inner and outer membranes, while the final explosion corresponds to the sudden loss of integrity of the cell wall by action of the endolysins[33].

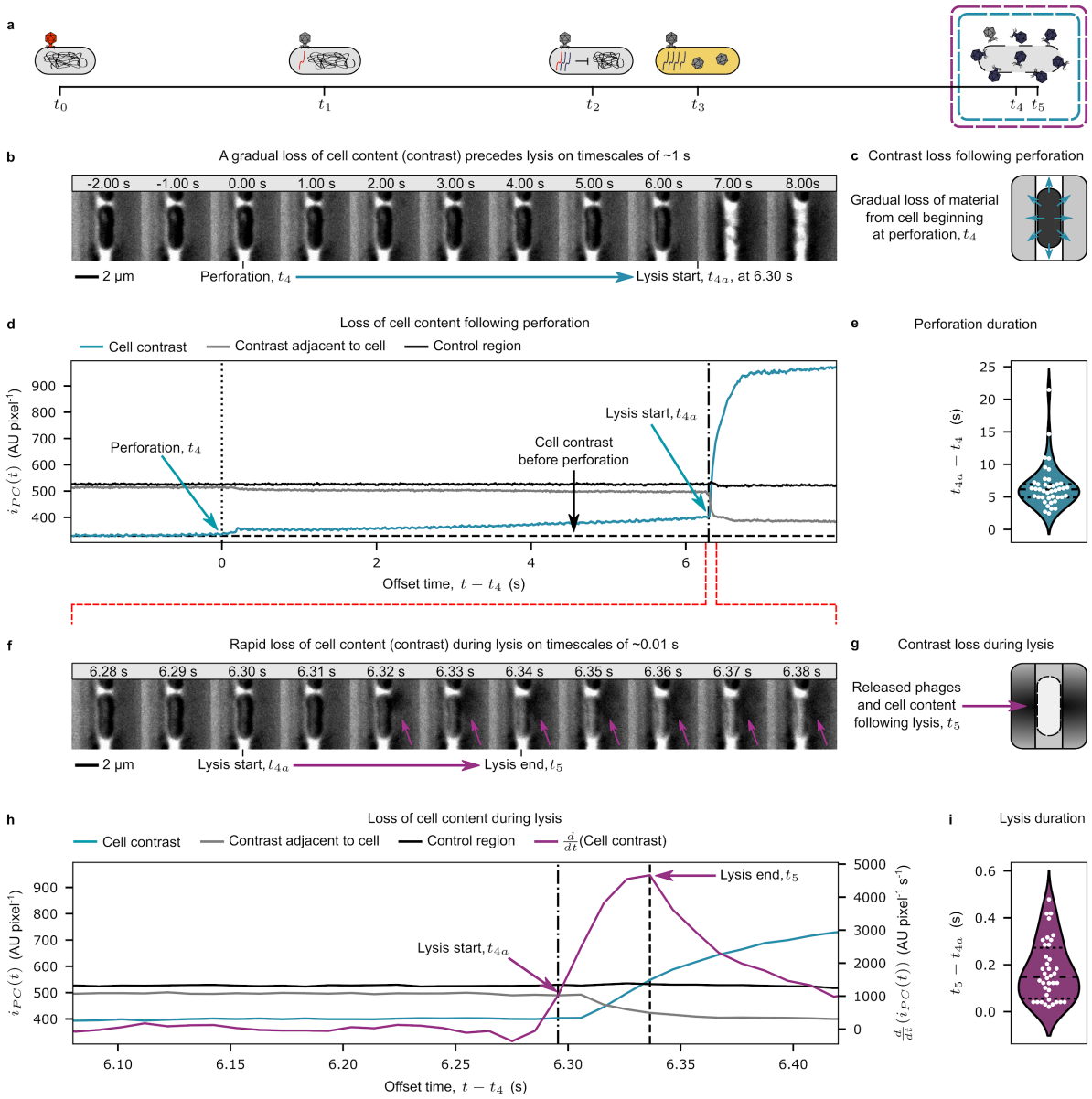

Fig. 4: High frequency imaging reveals that T7 induced lysis occurs in two phases
a. A timeline of the T7 phage life cycle, indicating the timing of perforation (t_4) and lysis (t_5). **b.** A kymograph showing the cell lysis on timescales of 1.00 s. The time axis is offset such that perforation (t_4) starts at time zero. **c.** A schematic illustrating the gradual loss of material from the cell which follows perforation and gives a loss of contrast in the images. **d.** Time series data showing the phase contrast intensity within and outside the cell shown in the kymograph in (b). **e.** Violin plot showing the distribution of perforation duration across different infection events (perforation to lysis start, t_4 to t_{4a}). The mean perforation duration is 6.57 s (n = 41, CV = 51%). The central dashed line represents the median and the outer dashed lines the first and third quartiles. **f.** A kymograph showing the cell lysis event seen in (b) and (d) on timescales of 0.01 s. Arrows indicate the rapid ejection and subsequent dissipation of a large amount of material from the cell. **g.** A schematic illustrating the total contrast loss of the cell, and the contrast increase in the adjacent side trench due to the released cell debris, which follows lysis. **h.** Time series data showing the phase contrast intensity and within and outside the cell shown in the kymograph in (f). The rate of change of

contrast loss within the cell is also plotted. Material loss proceeds steadily from the initial perforation (t_4) for 6.30 s, before the rate suddenly starts to increase (t_{4a}). We declare lysis complete (t_5) when the rate of contrast loss reaches a maximum, which happens 0.04 s after the sudden increase starts at t_{4a}. **i.** Violin plot showing the distribution of lysis duration (lysis start to lysis end, t_{4a} to t_5). The mean lysis duration is 0.17 s (n = 38, CV = 73%). The central dashed line represents the median and the outer dashed lines the first and third quartiles.

Heterogeneity in lysis time is driven by variability in the early stages of infection

Having measured the timing of several points in the infection cycle, we set out to construct a full timeline of the typical T7 infection cycle, alongside a comparison of the relative contributions to the overall variability in lysis time of each individual infection step.

Fig. 5a illustrates a comprehensive timeline of the typical infection cycle of T7 on *E. coli* cells, from phage adsorption onto the cell to the mean of four key time points in the infection cycle: genome injection (t_1), host cell shutdown (t_2), capsid expression (t_3), and cell lysis (t_5). Error bars accompany each time point, representing the range of variability (± standard error of the mean). The perforation step (t_4) is not represented here due to its negligible duration compared to the other stages.

Analysis of this timeline reveals that genome injection typically concludes 5.6 min after phage adsorption, accounting for just under one third of the overall lysis time (18.6 min). Approximately 8.7 min into the infection cycle, the host cell ceases growth, then capsid production starts at 10.4 min after adsorption (just over halfway through the infection cycle). Approximately 8.2 min thereafter, the cell undergoes lysis, releasing the phage copies into the surrounding environment. The average duration from adsorption to lysis is 18.6 min, consistent with the value obtained from bulk experiments (methods). The CV is 15.3% across infection events.

We illustrate the noise in timing between various points in the infection cycle and lysis in Fig. 5b. Here, all time points are directly measured with reference to cell lysis, as this is the most sudden and clearly identifiable of the events. We find that the noise in the overall lysis time is comparable to the noise in the time interval between the end of injection to lysis. Conversely, the durations between growth arrest, capsid production start, and lysis exhibit high consistency, with interquartile ranges spanning just 1.5 min. These data suggest that the primary sources of variability in lysis time stem from the initial stages of infection up to the point in which cell growth stops. After this point, which delineates the time when the phage has likely taken control of the host molecular machinery, the timing of events is remarkably consistent across infection events.

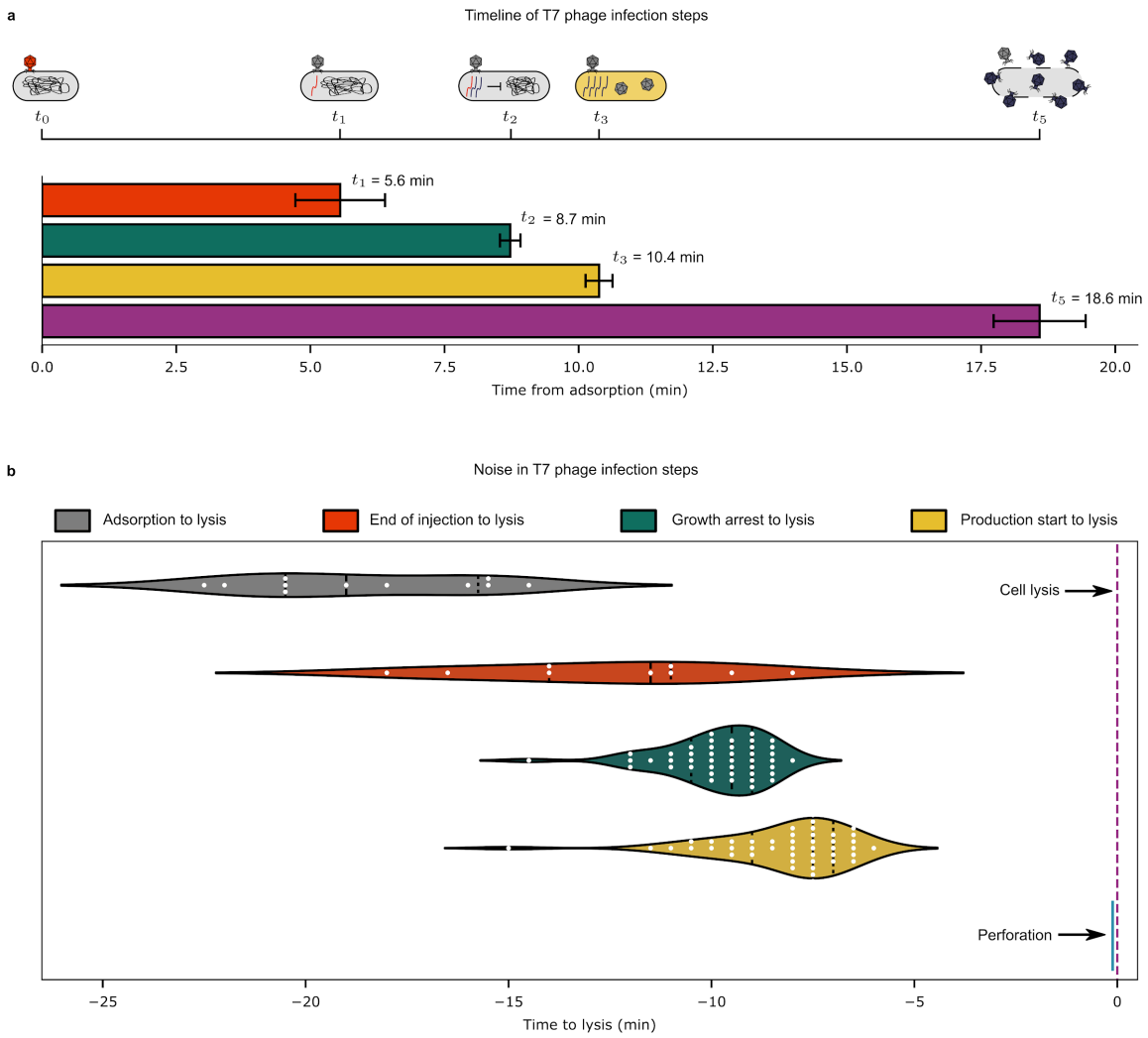

Fig. 5: The timing of individual steps of infection and the associated variability across events

a. Timeline of phage infection steps. Each bar represents the mean time from adsorption to the indicated time point in the T7 phage life cycle. The error bars are ± the standard error of the mean. Sample sizes for the measurement of t_1 (injection end), t_2 (growth arrest), t_3 (production start) and t_5 (lysis) are 9, 45, 45 and 11 respectively. **b.** Kernel density estimates of the timing distributions from different time points in the T7 phage life cycle to lysis. Each single-cell infection event measured is shown as a white dot. Inner and outer dashed lines in each violin represent the median and lower and upper quartiles respectively. Adsorption to lysis (grey violin) has mean 18.6 min, n=11. Injection end to lysis (orange violin) has mean 12.6 min, n=9. Growth arrest to lysis (green violin) has mean 9.9 min, n=45. Production start to lysis (yellow violin) has mean 8.2 min, n=45. The perforation to lysis time is represented as a solid blue line, as relative to the timescales of the other steps, the contributed noise from this step is negligible (the mean is 0.11 min, CV = 52%, n=36).

Lysis time variability can provide fitness advantages to phage populations

Lysis time represents a key life history parameter for lytic phages and is known to be under strong selective pressure in laboratory experiments[32,34–37] and potentially in the wild. Its fitness effect on phage populations in different environments is theoretically well studied, however, due to the lack of experimental data regarding its level of stochasticity, it is typically assumed to be either noiseless or exponentially distributed for modelling convenience[38–41]. Our data provide the unprecedented opportunity to quantify lysis time variability, raising the question of whether it can represent an evolutionary trait conferring a fitness advantage to a phage population.

To investigate this question, we used stochastic agent-based simulations of a serial passage experiment, in which two phage populations, denoted as “wild type” and “mutant”, are initially mixed in equal proportion and then passaged through several population bottlenecks until one phage approaches fixation (Fig. 6a, methods). The wild type and mutant phage share the same burst size distribution, but have distinct and inheritable lysis time distributions. Some examples of these distributions are shown in Fig. 6c. Mutant 1 has the same mean lysis time as the wild type, but different standard deviation. Mutant 2 has the same mean and standard deviation in lysis time as the wild type, but different skew.

Fig. 6d shows the probability of mutant fixation as a function of standard deviation (mutant 1, left panel) and skew (mutant 2, right panel) determined over 25 independent simulations. The results show that a larger standard deviation confers a fitness advantage, if mean and skew are the same, while a negative skew in lysis time is advantageous when the mean and standard deviation are the same. Overall, our results clearly indicate that the mean lysis time alone is not sufficient to predict phage fitness, and the higher order moments of the distribution can significantly alter a phage’s competition advantage.

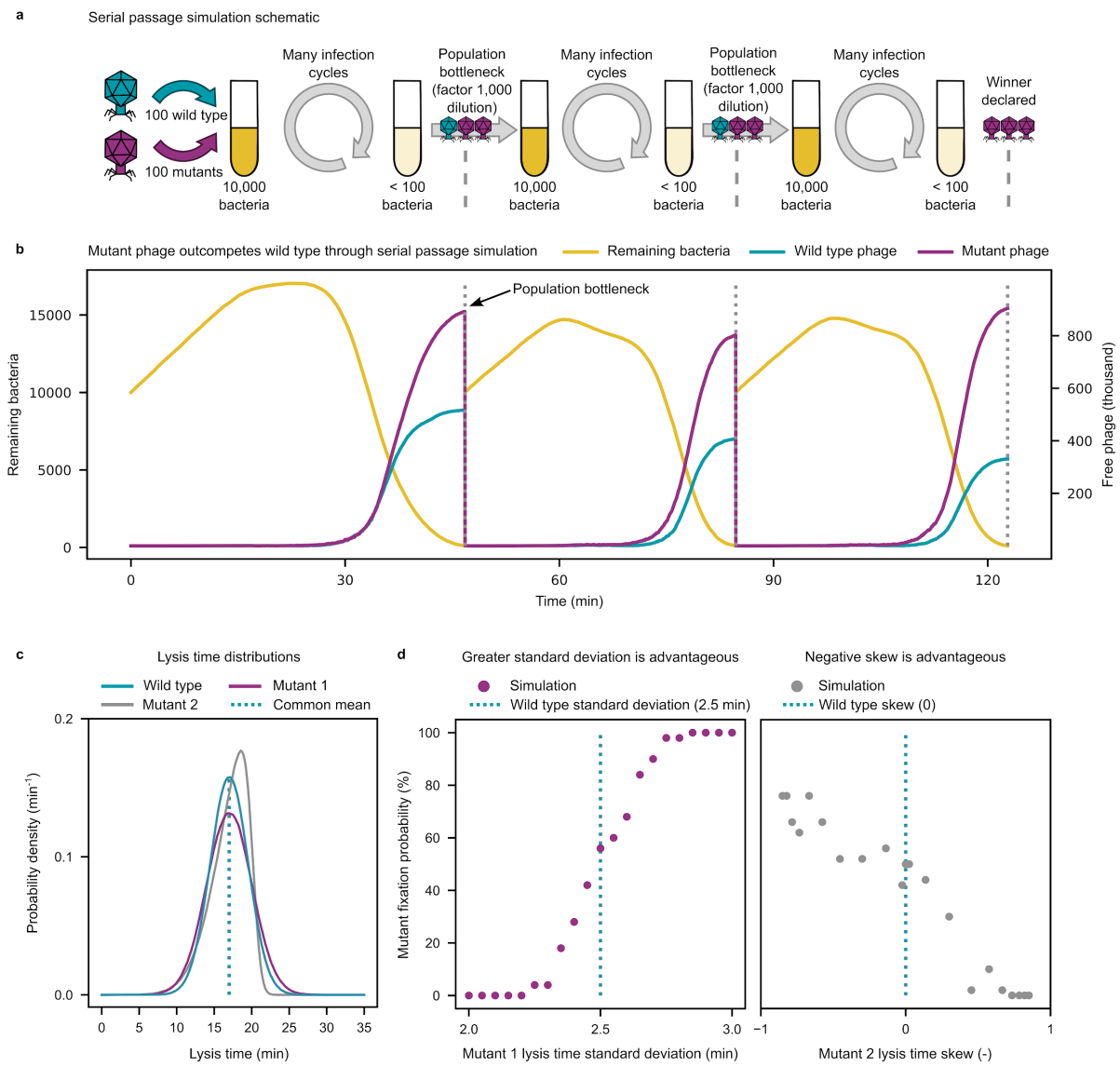

Fig. 6: Simulations predict lysis time variance and skewness impact phage fitness
a. A schematic explaining the serial passage simulation, where a wild type and mutant phage with lysis times drawn from different distributions (Fig. 6c) compete and undergo several rounds of dilution into fresh bacteria. A full explanation of the simulation can be found in the methods section. **b.** Example time series data from the simulations, demonstrating the growth and lysis of the bacteria (yellow line), and the proliferation of the wild type and mutant phage (blue and purple lines respectively). At the population bottleneck, a 1000 fold dilution of the phage into fresh bacteria is simulated. If, after a bottleneck, one phage forms >70% of the total phage population, it is declared the winner. **c.** Example lysis time distributions of wild type and mutant phage. Mutant 1 has the same mean as the wild type, but the standard deviation in lysis time is varied (Fig. 6d, left panel). Mutant 2 has the same mean and standard deviation as the wild type, but the skew in lysis time is varied (Fig. 6d, right panel). **d.** When competing against a wild type phage, mutants with lysis times drawn from a distribution with equal mean but greater variance are predicted to have a fitness advantage (left panel). Mutants with lysis times draw from a distribution with equal mean and variance to the wild type but with negative skew are also predicted to have a fitness advantage (right panel). Each data point is computed from 25 simulations.

Discussion

Here, we have reported the first study that quantifies the kinetics of individual steps in the lytic cycle of phage T7 at single phage-single cell resolution. Our novel assay provides a new way to quantify phage-bacteria interactions that is orthogonal to omics analyses, which provide dynamic but averaged phenotypes, and structural investigation, which assess variability but are based on static observations. Our approach enables dynamic measurements across many infection events, while maintaining the individuality of each of them in order to assess variability and correlations across the phenotypes of the phage and the corresponding infected cell.

We find that the major source of variability in the timing of infection events comes from the early steps of viral DNA entry up to cell growth arrest, while the second part of the infection process, between host take-over and cell lysis, is remarkably robust. A possible explanation for this difference is that the initial steps of infection rely on low copy-number molecules, such as one viral genome, or an initial few copies of T7 RNAP, which are subject to large relative number fluctuations. However, we cannot exclude that variability in the structural properties of the capsid[42] and consequent attachment to the host cell receptors might contribute to what we observe. Future studies that quantify the proportion of unsuccessful adsorptions on one side, and the spatial dynamic of the T7 RNAP within the infected cell, on the other, will help answer this question.

The second phase, in which capsid proteins and, arguably, viable phage particles are produced within the host cell, exhibits a surprisingly large variability in kinetics and final amount, despite the robustness in the timing of the events. The strong correlation between the total protein production and the size of the growth-arrested host suggests that this variability may originate in physiological differences across infected cells. Indeed, we find that the phage protein production rate strongly depends on cell size, highlighting that the process heavily relies on host cell resources, such as ribosomes and cellular energy, which scale with cell size. The positive correlation between production start to lysis time and cell size is less clear and even counterintuitive given our current knowledge of what triggers cell lysis[30,31]. Further analysis of the ultra-fast imaging data of lysis events and perturbations to the cell metabolic state may shed light onto currently unidentified processes that contribute to lysis.

Accurate quantification of the sources of phenotypic variability and their relative correlations across infection events is not only important to understand the underlying molecular mechanisms controlling phage infection outcomes, but can also have significant evolutionary consequences. Our simulation results clearly show that mean phenotypic values, such as average lysis time, are insufficient to predict the fitness advantage of a phage population and that higher moments of the distribution can have a significant impact. These findings open the intriguing and currently unexplored possibility that variability in phage phenotype could be under strong selective pressure, raising fascinating questions regarding how evolution shapes it in different scenarios.

Finally, although this work has primarily focused on T7-*E. coli* to benchmark the assay using a well-studied model system, the approach can readily be applied to any natural, evolved, or

engineered phage. The high-throughput and scalable nature of the platform can be harnessed for multiplexity, to benchmark a variety of sequence variants of phages against specific target bacteria or multiple mutants of a target bacteria against a particular phage. Precise characterisation of properties associated with infection steps (such as adsorption, production, and lysis) can generate a multi-phenotypic profile for each phage-bacteria pair, enabling detailed analysis of mechanisms underlying response, resistance, and phage-bacteria co-evolution. Similarly, a collection of natural or engineered phages can be evaluated for their efficacy in eradicating a target strain, with implications for medical or biotechnological applications. In summary, this assay promises to open up new avenues for the systems analysis of phage-bacteria interactions and their practical applications.

Online Methods

Bacterial strains and growth conditions

The following bacterial strains were used in this study.

Table 1: List of *E. coli* strains used in this study

Name	Species	Genotype	Use
SB8	*E. coli*	MG1655 7740 Δ*motA*	Experiments for Figs. 1 to 5.
SB7	*E. coli*	SB8-*glmS*::PRNA1-mCherry -mKate2	Training data for cell segmentation.
MI13	*E. coli*	MG1655 6300 attTn7::PrpsL-mCherry-mKate2	Microfluidic device optimisation experiment.
BW25113	*E. coli*	BW25113	Generating phage lysates.

Prior to experiments in the microfluidic device, cells were grown overnight in a shaking incubator at 250 rpm and 37 ^{o}C in LB Miller (Invitrogen) containing 0.8 g L^{-1} of pluronic F-108 (Sigma, part number 542342). Cultures were started directly from a frozen stock to maintain a consistent genetic diversity across the cells used in experiments across different days. The LB Miller was sterilised by autoclaving. The pluronic F-108 was first prepared as a 100 g L^{-1} solution and filter sterilised, and then diluted 0.8 % v/v into the LB Miller.

Phage lysate preparation and PFU estimation

E. coli BW25113 strain cells were grown overnight in a shaking incubator at 250 rpm and 37 ^{o}C in LB Miller (Invitrogen). 500 µL of the overnight liquid culture was used to inoculate 20 mL volume of LB Miller and left to grow in a shaking incubator at 37 ^{o}C for 1 h 40 min. Once the culture reached OD 0.6-0.7, 500 µL of stock phage lysate was added and left in the shaking incubator for 7 min. The phage-inoculated cells were centrifuged in a pre-chilled (4 ^{o}C) centrifuge at 5000 rpm for 5 min. The supernatant was discarded and the pelleted cells

were resuspended in 2 mL of fresh LB Miller. The resuspended culture was left in the shaking incubator for 1 h at 37 °C for the infected cells to fully lyse. The lysate was aliquoted in 1.5 mL Eppendorf tubes and centrifuged at 14000 rpm for 10 min. The resulting supernatant was passed through 0.22 µm filters to remove any traces of cell debris and unlysed cells. The number of plaque forming units (PFU) in the filtered lysate was estimated using a plaque assay. For this, serial dilutions of the filtered lysate were set up ranging from dilution factor 10^5 to 10^8. 20 µL of each diluted lysate was mixed with 100 µL of overnight BW25113 cells in 5 mL of 0.7% agar LB, kept at 50 °C. The mixture was briefly vortexed and poured as a thin layer of agar on 9 cm-diameter plates and incubated at 37 °C for 4 h. The formed plaques were counted and the number divided by 20 to estimate the number of PFU per µL of each dilution factor. Measurements across three dilution factors were used to estimate the concentration of PFUs per µL of the filtered lysate. The titres of lysates used for experiments in this study were measured as follows:

Table 2: List of T7 strains used in this study

Experiment	Strain	PFU
Figs. 1, 3, 5	TY009, Sytox Orange labelled	1.0×10^7 µL^{-1}
Fig. 2	WT T7, Sytox Orange labelled	3.5×10^7 µL^{-1}
Fig. 4	WT T7, unlabelled	4.0×10^7 µL^{-1}

Filtered lysate was used either directly or stained as per the protocol below. Note that lysate titres listed in Table 2 are diluted into growth media during microfluidic experiments.

Genetic engineering of phage: construction of TY009

Wild type T7 genomic DNA was extracted from a fresh lysate preparation (see Lysate Preparation protocol) using Norgen Genomic DNA extraction Kit (Norgen, SKU 24770), following manufacturer's instructions. The WT genomic DNA was used as a template for Q5® High-Fidelity 2X Master Mix (NEB, M0492L) PCR reactions to clone three fragments of the T7 genome, as well as the phi10:mVenusNB insert using the oligos listed in Table 3. The template for the *E.coli* codon-optimised mVenusNB insert was ordered as a gene block from IDT. The circularisation fragment was ordered as a pair of oligos from NEB and was annealed prior to their use in the DNA assembly reaction.

Table 3: List of oligo sequences

Fragment	**Oligo forward sequence**	**Oligo reverse sequence**	**Fragment length**	**Melting temperature**
Fragment 1	TCTCACAGTGTACGGACCTAAAGTTCCC	GTCGTTGGACCAGTCTGTTGACTCTG	13253	72
Fragment 2	CAGACTGGTCCAACGACACTGACTTC	CTTCTGGGCGAAGACCACCGTG	10737	72

phi10:mVenus NB insert	TGGTCTTCGCCCAGAAGCTGCTGGTGCAGTGGTTTTCAAAGTG	GAGGCCCCAAGGGGTTATGCTAGTTATTTGTAGAGCTCATCCATGCCATGGG	1040	72
Fragment 4	TAACCCCTTGGGGCCTCTAAACG	AGGGACACAGAGAGACACTCAAGGTAAC	15769	72
Circularisation fragment	GAGTGTCTCTCTGTGTCCCTGGTACCGCTCGTGAGGGCACTCTCACAGTGTACGGACCTA	TAGGTCCGTACACTGTGAGAGTGCCCTCACGAGCGGTACCAGGGACACAGAGAGACACTC	60	-

The Q5 Master Mix was supplemented with 0.5 µL of 10 µM DNTP's solution and the extension time was set to 13 min. The cloned fragments were purified using the Monarch® PCR & DNA Cleanup Kit (5 µg) (NEB, T1030L) and the DNA concentration was measured using Qubit 4 Fluorometer (Invitrogen). The fragments were assembled in a NEBuilder® HiFi DNA Assembly Master Mix (NEB, E2621L), as per manufacturer's recommended ratios and incubated at 50 ºC for 1.5 h. 10 µL of the reaction product was used to transform an aliquot of electro-competent cells using the MicroPulser Electroporator (BioRad). The cells were pulsed 3 times to ensure the integration of the circularised phage genome within the cells. The electroporated cells were immediately supplemented with 1 mL of room temperature LB Miller and left in a shaking incubator at 37 °C for 1 h. The resulting lysate was diluted serially up to dilution factor of 10^4 and all dilutions were used in a plaque assay. The plaques were screened under a microscope and YFP-expressing plaques were individually cored out and dissolved in 50 µL of fresh LB. These phage suspensions were used to prepare concentrated lysates from which genomic DNA was extracted. DNA extracted from candidate plaques was fully sequenced by Plasmidsaurus to confirm correct scar-free integration of the phi10:mVenusNB insert and absence of any mutations from the template WT T7 genome.

Staining the DNA of the phage genome

The genomic DNA of the T7 phage was stained with the DNA binding dye SYTOX Orange (Invitrogen, S11368). To reduce the bacterial DNA background, the concentrated phage lysate was incubated at 37 ºC with DNase I-XT (NEB M0570L), for 1 h. Such treatment did not significantly reduce the titre of PFUs (No treatment - 2.25 x 10^7 PFUs μL^{-1}; DNAse I-XT treatment alone - 2.05 x 10^7 PFUs μL^{-1}; SYTOX Orange treatment alone - 1.00 x 10^7 PFUs μL^{-1}; DNAse I-XT and SYTOX Orange treatment - 1.00 x 10^7 PFUs μL^{-1}) but significantly reduced the background fluorescence from dyes bound to DNA fragments from lysed cells. The treated lysate was then stained with SYTOX Orange at a final concentration of 2.5 µM and left overnight at 4 ºC. Excess dye was removed by centrifuging the stained lysate across a 100 kDa (Amicon® Ultra, UFC5100) filter and rinsing the dye away across the filter membrane with fresh LB four times. The concentrated stained phages were resuspended in 1 mL of fresh LB and stored at 4 ºC.

Population level measurement of lysis time

Population level measurements of the mean lysis time of wild type T7 and TY009 were carried out according to the 'one-step growth curve' or 'lysis curve' protocol[43]. An overnight culture of SB8 (Table 1) was diluted 1:100 into 1 ml of fresh LB Miller (Invitrogen) and placed in a shaking incubator at 37 °C, 250 rpm. After 2 h this culture was inoculated with 1 µl of bacteriophage stock, kept at 5 °C. At the same time, a second 1:100 dilution of the overnight culture was made, and both cultures were incubated for 2 h, yielding one dense bacterial culture (order 10^8 cells ml^{-1}, OD_{600} of 0.8), still in exponential phase, and one clear culture with few remaining cells but a very high density of bacteriophage (order 10^{10} PFUs ml^{-1}). Both cultures were transferred to centrifuge tubes and spun at 6,000 g for 5 min. In the bacterial culture, the supernatant was removed and the pellet of cells was resuspended in 1 ml of fresh LB. In the phage culture, the supernatant was transferred to a new tube and any pellet of cell debris was discarded.

At time t = 0, the cell culture was inoculated with 10 µl of bacteriophage culture, vortexed, and placed in a bench-top shaking incubator at 37 °C, 300 rpm. The remaining bacteriophage culture was discarded. 1 min was allowed for adsorption to take place, after which the culture was serially diluted down to two 'active' cultures 'D6', and 'D7', corresponding to dilution factors of 10^6 and 10^7 respectively. D6 and D7 were kept in the bench-top incubator (37 °C, 300 rpm) , with 20 µl samples taken of each every 2.5 min and the bacteriophage density determined by plaque assay (see PFU estimation in methods).

The population-level mean lysis time was determined by fitting a Gaussian cumulative distribution function to the data. In some experiments, the number of PFUs was observed to decay after the step, which may be due to multiple virions adsorbing to the same bacterial cell, thus concealing their true number. In these cases, the dataset was truncated after the step. Three replicates were carried out for each bacteriophage, each on a different day starting from a different clonal population of bacteria.

The three lysis times measured for wild-type T7 were 16.7 min, 13.8 min, and 13.9 min, giving a grand mean and standard deviation of 14.8 ± 1.3 min. The three lysis times measured for TY009 were 18.6 min, 22.9 min, and 18.8 min, giving a grand mean and standard deviation of 20.1 ± 2.0 min. The measured values for both phages agree to within the experiment's 2.5 min resolution.

Microfluidic device fabrication

The microfluidic devices were fabricated using soft lithography, by casting a silicone elastomer onto a silicon wafer. We received this wafer as a gift from Dr. Matthew Cabeen of Oklahoma State University. It was fabricated by the Searle Clean Room at the University of Chicago (https://searle-cleanroom.uchicago.edu/) according to the specifications provided by Dr. Cabeen and his colleague, Dr. Jin Park. These specifications were based on the design presented by Norman *et al.*[18]. The silicone elastomer was prepared by mixing polydimethylsiloxane (PDMS) and curing agent from the Sylgard 184 kit (Dow) in a 5:1 ratio and degassing for 30 min in a vacuum chamber. The elastomer was then poured onto the silicon wafer and degassed in a vacuum chamber for a further 1 h. The elastomer was then cured for 1 h at 95 °C. The appropriate devices were then cut out and inlet and outlet holes

were punched with a 0.75 mm biopsy punch (WPI). Devices were then cleaned with Scotch Magic tape before being sonicated in isopropanol for 30 min, blow dried with compressed air and then sonicated in distilled water for 20 min. 22x50 mm glass coverslips (Fisherbrand) were sonicated for 20 minutes in 1 M potassium hydroxide, rinsed and then sonicated for 20 min in distilled water before blow drying with compressed air. The devices and coverslips were then dried for 30 min at 95 °C. Devices and coverslips were plasma bonded using a Diener Electronic Zepto plasma cleaner, by first pulling a vacuum to 0.1 mbar, and then powering on the plasma generator at 35% and admitting atmospheric air to a chamber pressure of 0.7 mbar for 2 min. Device and coverslip were then bonded and heated on a hotplate at 95 °C for 5 min, before transferring to an oven at 95 °C for 1 h to produce the finished microfluidic devices.

Single cell infection assay

On the day of the experiment, sterile growth media containing LB Miller (Invitrogen) with 0.8 g L^{-1} pluronic F-108 (Sigma-Aldrich) was loaded into a syringe. The pluronic is added as a surfactant to prevent cell clumping in the overnight culture, to improve cell loading, and to prevent cells clumping at the outlet of trenches. It is added to the media at sub-inhibitory concentrations[12]. The lane of the microfluidic device to be loaded was first passivated by adding the above described growth media into the lane with a gel loading tip, and allowing it to rest for 10 min. A 1 mL volume of the cells grown overnight were transferred into a 1.5 mL tube and spun gently at 1000 g for 3 min to sediment the cells. The supernatant was poured away and the cells resuspended in the residual volume. A small volume of this dense cell culture was then pushed into the passivated lane using a gel loading tip and left to rest for 10 min. During this time, the small stationary phase cells will diffuse into the trenches.

While the cells are diffusing into the trenches, growth media from the syringe is pushed through a silicone tubing path to purge the tubing of air. The tubing has a forked path, and the flow is directed down a given fork using a 3-way solenoid pinch valve (Cole Parmer). One fork supplies the microfluidic device with growth media, while the other leads directly to the waste bottle.

The media flow is then connected to the lane of the device containing the cells using 0.83 mm outer diameter needles. The outlet flow goes to a waste bottle. Inlet flow from the media syringe is driven by a syringe pump, and initial flow is set to 100 μL min^{-1} for 10 min to clear excess cells from the lane. Media flow is then reduced to 5 μL min^{-1}. Following this, 365 nm illumination light is shone onto the inlet of the device such that each part of the inlet receives at least 7 min of illumination. This kills any cells not removed by the high flow rate, and helps to prevent biofilm formation in the device inlet.

The cells are grown in the device for a minimum period of 3 h from the introduction of fresh growth media into the lane, to allow the cells to reach a steady state, exponential growth phase. After this wake up period, the media is switched to media containing phage to begin the infection imaging. A typical phage media composition is described in Table 4, which would result in a final phage titre of 10^6 PFU μL^{-1}. Note that the phage lysate is also washed and resuspended in LB Miller, so the exact lysate volume used is unlikely to significantly change the nutritional composition of the media.

Table 4: Phage treatment media composition

Component	Volume (µL)	Volume fraction (-)	Concentration in media
LB Miller	4460	0.892	N/A
Pluronic F-108, 100 g L^{-1}	40	0.008	0.8 g L^{-1} pluronic F-108
Phage lysate, PFU 10^7 µL^{-1}	500	0.100	10^6 PFU µL^{-1}
Total	5000	1.000	N/A

The phage titre must be sufficiently high to ensure at least some infections occur in each given trench, but the exact titre is unimportant in the ranges used, as almost all first round infections result from just one phage binding to a cell.

To change the media to phage media, the solenoid pinch valve is activated to block flow to the microfluidic device. The flow to the microfluidic device is blocked for a maximum of 10 min. While it is blocked, the growth media syringe is changed to a syringe containing growth media with phage, and then the tubing is flushed with the phage media at high flow rates, such that the growth media without phage is completely cleared from the tubing. Then, the flow rate is returned to 5 µL min^{-1} and the flow is switched to introduce phage media to the cells. Purging the initial section of tubing with phage media reduces the time between the switch and the phages reaching the cells, without having to expose the cells to high flow rates which could cause mechanical stress. Additionally, it purges bubbles which can sometimes be introduced when the syringes are switched.

Once the media is switched, time-resolved image acquisition begins.

Microfluidic device design optimisation

To investigate the effect of trench design on the access of phage to the cells, we carried out a parallel infection assay across two trench designs, one with side trenches, and one without.

The method used was similar to that described above (methods, single cell infection assay). MI13 cells (Table 1) were grown in the trenches of both devices. The growth media used was LB Lennox (Invitrogen), with an addition of 1% v/v of sterile filtered 100 g L^{-1} pluronic F-108 (Sigma-Aldrich) solution. Cells were first grown in this media for 8 h at a flow rate of 20 µL min^{-1}. Media containing phage was prepared to be the same as the growth media, but with the addition of 1.5 x 10^5 PFU µL^{-1} of T7 phage. The phage used was based on T7 Select 415-1 (Merck, https://www.merckmillipore.com/GB/en/product/T7Select-415-1-DNA,EMD_BIO-70040), with an mEYFP protein under the control of the T7 pPhi10 promoter inserted into the designated insert region, just downstream of gene 10. The cells were imaged in red fluorescence, yellow fluorescence and phase contrast every 4 min during the course of the infection using a Plan Apo λ 100x Oil Ph3 DM objective (see methods, time resolved image acquisition for microscopy details).

The results of this comparative infection assay demonstrate that side trenches are necessary to facilitate the initial infection and subsequent trench clearance from the following rounds of lysis. We judged a cell to be infected if there was a visible yellow signal in the cell. The fraction of trenches showing any infection over the course of the experiment was 98% for trenches with side trenches, but only 13% for the trenches without sides (n=53 for trenches with sides, n=56 for trenches with no sides). Similarly, in 98% of the trenches with sides, all cells were lysed by phage, but for the trenches without sides, there were no trenches where all cells were lysed. These results demonstrate that phage have greater access to cells when the side trenches are used, and also that initial lysis events can lead to successful second rounds of infection in the side trench devices, leading to complete clearance of cells from the trenches.

Time-resolved image acquisition

Images were acquired using a Nikon Eclipse Ti2 inverted microscope with a Hamamatsu C14440-20UP camera. The microscope has an automated stage and a perfect focus system, which automatically maintains focus over time. The microscope contains two multiband filter cubes, each of which contains a multi-bandpass dichroic mirror and corresponding multiband excitation and emission filters. There is an additional emission filter which can be quickly switched to select the correct emission wavelength band. Together the multiband cubes and the emission filter wheel allow for fast imaging in multiple colour channels. All captured images are initially saved using Nikon's ND2 file format. For the experiments in Figs. 1, 2, 3 and 5, imaging began before the phage media reached the cells, and continued at a regular frequency for the duration of the experiments.

To image the cell lysis at very high time resolution (Fig. 4), the imaging interval was set to 10 ms (100 frames s^{-1}). The camera manufacturer claims a maximum frame rate of 100 frames s^{-1} using a region of interest (ROI) set to 2304 × 2048 pixels. However, we found that a frame rate close to 100 frames s^{-1} could only be achieved when the ROI was considerably smaller, and only included one trench. The exposure time for this imaging was 3 ms, as longer exposure times caused a reduction in the frame rate, and shorter exposures reduced the image contrast. Using these settings, we were able to achieve an imaging interval of 10.2 ms. To image the short time period over which lysis takes place at such high time resolutions, it was necessary to be selective about when and where to image. We achieved this by seeing when a first lysis had occurred in a trench, and widespread growth arrest indicated an impending second round of lysis in the same trench. An ROI was drawn around such trenches, and high time resolution imaging was started to capture the lysis events.

The microscope settings used for each channel are listed in Table 5 below.

Table 5: Imaging settings for different experiments used in this paper

Experiment	Channel	Light source	Filter cube	Emission filter band centre/ band width (nm)	Objective	Imaging interval (s)

Figs. 1, 3, 5	Yellow	514 nm	LED-CFP/YFP/mCherry-3X3M-A	540/21	Plan Apo λ 100x Oil Ph3 DM	30
Figs. 1, 3, 5	Orange	561 nm	LED-DA/FI/TR/Cy5-B	595/40	Plan Apo λ 100x Oil Ph3 DM	30
Figs. 1, 3, 5	Phase contrast	Köhler	LED-CFP/YFP/mCherry-3X3M-A	540/21	Plan Apo λ 100x Oil Ph3 DM	30
Fig. 2	Orange	561 nm	LED-DA/FI/TR/Cy5-B	595/40	Plan Apo λ 100x Oil Ph3 DM	10
Fig. 2	Phase contrast	Köhler	LED-DA/FI/TR/Cy5-B	515/30	Plan Apo λ 100x Oil Ph3 DM	10
Fig. 4	Phase contrast	Köhler	LED-DA/FI/TR/Cy5-B	515/30	Plan Apo λ 100x Oil Ph3 DM	0.01

Image preprocessing

All captured images were pre-processed before feature extraction. First, individual frames from the Nikon ND2 format were extracted and saved as PNG files using custom Python code which makes use of the nd2 module (https://pypi.org/project/nd2/). Using custom Python code (https://github.com/georgeoshardo/PyMMM), these frames were then registered to correct for any stage drift and rotated to ensure the trenches were vertical in the images. We then use automated methods to find the position of each trench in the images and crop out the trenches for further processing, as described below.

Cell segmentation

The phase contrast images of cells in the extracted trench images from our experiments in Figs. 1, 3 and 5 were segmented using a custom trained Omnipose machine learning model[44]. The model was trained on images (taken on a different day) of SB7 *E. coli* (Table 1) growing in our device where both fluorescence and phase contrast images were acquired using the same objective as for the experiments. These images will be referred to as training images, and are separate from the experiment image data.

To train the model, our approach was to first train an Omnipose model to segment fluorescence images. To generate a high volume of training data and corresponding ground truth masks for fluorescence images of cells in the mother machine, we use a virtual microscopy platform called SyMBac[20]. Using this fluorescence model, we segmented fluorescence images of cells and generated cell masks for the fluorescence channel of the training images.

The cell masks for the fluorescence channel were then checked against the phase contrast training images, and pairs of fluorescence masks and phase contrast training images which matched well were manually curated into a training data set. This training data was used to train an Omnipose model for the segmentation of phase contrast images. The phase contrast model was then used to generate cell masks for the experiment image data.

Feature extraction

Basic cell properties, such as cell position, length, area, and YFP intensity, were extracted from regions of the images corresponding to the cell masks produced by segmentation. The cell properties were extracted using custom Python code utilising the scikit-image regionprops function[45].

For the data in Fig. 3, further properties are calculated from the basic cell properties. Mathematical descriptions are found in Table 6. To calculate the cell growth rate, $\lambda(t)$, for a given cell, we first calculated the natural logarithm of the cell length in μm. Then, we used a Savitzky-Golay filter[46] with a third-order polynomial and a window size of eight data points to smooth the signal. The growth rate was calculated as the first derivative of this smoothed signal (the difference between sequential data points divided by the imaging interval). To calculate the time of growth arrest, an average, uninfected growth rate was calculated from 75 uninfected cells (0.0304 min^{-1}). A threshold growth rate for growth arrest was then set as half this value. We declare growth arrest (t_2) as the first point where the growth rate drops below this threshold, if the growth rate remains below this threshold for a minimum of four consecutive time points.

The growth arrested cell length, L_{GA}, is calculated as the mean cell length between growth arrest, t_2, and the penultimate length measurement before lysis. The final length measurement prior to lysis is not included in the calculation, as the final measurement is susceptible to sudden length changes which may occur if the image is captured just prior to lysis. Any such changes would not be representative of the cell size throughout the infection period, which otherwise remains approximately constant.

Table 6: Properties of infected cells

Property	**Unit**	**Description**
Time, t	min	Time from the start of imaging.
Interval between frames, Δt	min	Time between consecutive frames. The values for each experiment are defined in Table 5.
Cell length, $L(t)$	μm	Cell length from scikit-image regionprops function.
Cell area, $A(t)$	pixel	Cell area from scikit-image regionprops function.
Raw total intensity of YFP, $I_{raw}(t)$	Arbitrary units (AU)	Sum of YFP pixel intensities over the cell area, from scikit-image regionprops function.
Raw mean intensity	AU $pixel^{-1}$	Mean of YFP pixel intensities over the cell area, from

of YFP, $i_{raw}(t)$		scikit-image regionprops function.
$\ln(L(t))$	-	Natural log transform of the cell length.
$[\ln(L(t))]'$	-	Result of applying the Savitzky-Golay filter[46] to $\ln(L(t))$ using a third-order polynomial and a window size of eight data points.
Growth rate, $\lambda(t)$	min^{-1}	$\lambda(t) = \frac{d}{dt}[\ln(L(t))]'$
Growth arrested cell length, L_{GA}	µm	$L_{GA} = \frac{\Delta t}{t_5 - 2\Delta t - t_2} \sum_{t=t_2}^{t_5 - 2\Delta t} L(t)$
Mean background intensity of YFP, i_{bg}	AU pixel^{-1}	The time series mean, over the time period prior to any YFP expression in each cell, of $i_{raw}(t)$.
Total background YFP intensity, $I_{bg}(t)$	AU	$I_{bg}(t) = i_{bg} \cdot A(t)$
Total intensity, background corrected, $I(t)$	AU	$I(t) = I_{raw}(t) - I_{bg}(t)$
Production rate, α	min^{-1}	$\alpha = \frac{1}{5} \sum_{t=t_3+2}^{t_3+4} \frac{d}{dt}[\ln(I(t))]$
Mean phase contrast intensity in a cell, $i_{PC}(t)$	AU pixel^{-1}	Mean of the phase contrast pixel intensities over the cell area, from the Fiji (ImageJ) function “Plot Z-axis Profile” over a hand drawn segmentation of the lysing cell.

The YFP capsid production reporter generates a fluorescence signal. For a given cell, the sum of pixel intensities from all pixels that fall within the cell outline gives the total intensity. We subtract the background intensity from the raw total intensity to give a total intensity, $I(t)$, as described in Table 6. The production start time, t_3, is calculated as the first time point when the total intensity reaches a value greater than 1420 AU, and then subsequently remains above that threshold for a total of four consecutive time points. This threshold was chosen by inspection as the intensity above which the total intensity would rise very rapidly, and below which was within the time series noise of total intensity.

The production rate of YFP was estimated by first calculating the instantaneous slope of the natural log transform of total intensity, and then finding the mean instantaneous slope in the window between 2 and 4 min after the production start. The window between 2 and 4 min was chosen as a representative production rate, as it happens close to the start of capsid production before saturation effects begin to take hold. Additionally, the total intensity values are sufficiently large 2 min after production start that the slope is less susceptible to the noise amplifying effect of taking the log transform of a noisy signal with a small magnitude (as $x \to 0$, $\ln x \to -\infty$).

For the high time resolution imaging of phage induced lysis (Fig. 4), a machine learning based approach for cell segmentation was unsuitable. This was because we wished to monitor the phase contrast intensity of the cell before, during and after lysis, so any attempt to segment the cells using features of the image would fail as those features changed. We therefore used a hand-drawn manual segmentation of a static region at the location of each cell in Fiji (ImageJ), as the cells did not move significantly over the short timescales of lysis. The mean phase contrast pixel intensity of this region, $i_{PC}(t)$, was then measured in each frame. By translating the static region by 1.43 μm to the left and right of the cell (along the short axis of the trench), the phase contrast intensities of the regions adjacent to the cell were also measured. By further translating the region on the right of the cell an additional 0.72 μm to the right and 4.29 μm along the long axis of the trench towards its closed end, a region in the side trench far away from the lysis was used as a control region for the phase contrast intensity.

Single cell lineage tracking

The single cell growth and lysis traces were tracked over time using features extracted at each frame, including cell position, area, orientation, and Zernike moments. This process was done using a custom Python script (https://github.com/erezli/MMLineageTracking). The algorithm predicts many potential states of these features for each cell at subsequent time steps. It then finds the best match to the feature states in the following frame to determine the tracking outcome. The results are stored in tree-structured Python objects containing detailed cell properties such as YFP mean intensity. The tracking results are visually checked using visualisation in kymographs.

Single phage tracking

To track the injection of the phage genome, the intensity of the bright spot indicating the location of the phage needed to be tracked over consecutive frames until the genome injection was complete. For the data in Fig. 2, the location of adsorption and injection events was determined with a semi-automated method using the Fiji (ImageJ) plugin Trackmate[47]. For the data in Figs. 1 and 5, an automated method was used to find injection events utilising the Python package Trackpy[48]. The two methods had similar efficacy in finding and segmenting bright spots, but Trackpy was automatable and allowed us to process the data faster. However, while both methods were good at finding and creating particle trajectories for the period while the phage was bright, neither method could consistently track the phage particle in the later stage of injection when the spot became very dim as most of the genome had already entered the cell.

Due to this, additional spot positions were estimated for the frames both before and after the segmented trajectory found by Trackmate or Trackpy ended. In the case of Fig. 2, spot positions before the segmented trajectory were estimated by assuming the spot velocity prior to the trajectory was equal to the mean spot velocity for the first half of the segmented trajectory. Similarly, spot positions after the segmented trajectory were estimated by assuming the spot velocity was equal to the mean spot velocity in the second half of the segmented trajectory.

For Figs. 1 and 5, the spot position needed to be tracked until cell lysis, as it was necessary to measure the YFP intensity to estimate the bleed through to the orange channel (see methods, correction of YFP bleed through). The position of the spot before and after the segmented trajectory was estimated by using a model of cell growth in the microfluidic device. Some of the estimated positions were then manually adjusted to ensure accuracy.

To measure the spot intensity, the mean of the brightest 28 pixels in a rectangular box centred on the spot position was computed for each frame. The box was made sufficiently long in the direction of the spot motion to account for any inaccuracies in the position estimation. Additionally, the mean of the brightest 28 pixels in a box alongside the spot box was computed to act as a control region. The measurements (along the short axis of the trench) of the spot and control box widths, along with the distance between the inside edges of these two boxes, are listed in Table 7. The spot and control box widths, along with the gap between the spot and control boxes, were larger for the experiment used for Figs. 1 and 5. This was because the trench width was larger, giving the cells more scope to change orientation between frames compared to the microfluidic device with a 1.0 μm trench width. Therefore, the box width was increased to ensure the phage spot remained within the box even if the cell moved in the direction of the short axis of the trench between frames.

The control distance was also larger for the experiment used for Figs. 1 and 5. This was because the signal from YFP proteins bled through into the orange channel where the cell was located. To generate a background signal free from bleed through interference, the control box had to be positioned in the side trench.

For Fig. 2, the time series spot intensity data was the time series of the brightest 28 pixels in the control box subtracted from the corresponding time series in the spot box. For Figs. 1 and 5, the time series spot intensity data was calculated as for Fig. 2, but an additional bleed through correction was applied to remove the bleed through into the orange channel from the YFP proteins (see methods, correction of YFP bleed through).

The duration of the genome injection was estimated by measuring the time between adsorption and the spot intensity returning to the intensity measured in the control box.

Table 7: Key parameters in the extraction of genome injection time series data

Experiment	Imaging interval (s)	Trench width (μm)	Spot and control box width (μm)	Gap between spot and control box (μm)	YFP bleed through
Fig. 2	10	1.0	0.65	0.325	No
Fig. 1, 5	30	1.4	1.43	0.91	Yes

Correction of YFP bleed through

The orange spot intensity, as described in the previous section, is initially reduced due to genome injection, but subsequently increases due to bleed-through from the production of YFP. While genome injection should generally be completed before YFP production starts, a

bleed-through correction was employed to reduce any effect of YFP production on the algorithmic detection of the completion of genome injection. To achieve this, the background-corrected orange phage spot intensity (orange signal) was first calculated as described in the previous section. Then, an identical method was applied to the yellow channel to obtain a background-corrected YFP signal from the same regions of the image.

From the YFP signal, an approximate production start time was calculated using the slope of the YFP signal. The YFP signal was first filtered using a Savitzky-Golay filter[46], with a third-order polynomial and a window size of eight data points. The first derivative of this filtered signal was then calculated to determine the slope. A threshold value for the slope was determined by first applying the Savitzky-Golay filter to the mean YFP intensity ($i_{raw}(t)$) of 75 uninfected cells and taking the first derivative of the filtered signal. The threshold value was set to be the mean plus three standard deviations of this slope, taken over the uninfected time period and the 75 cells. When the slope of the background-corrected YFP signal (the signal obtained in an analogous manner to the spot intensity in the orange channel) crossed this threshold for at least four consecutive time points, the production start time was declared at the point of first crossing.

A linear regression slope was then calculated between the production start time and lysis of both the background-corrected YFP signal and the background-corrected orange signal. A bleed-through coefficient was calculated as the ratio of the linear regression slope of the YFP signal to the linear regression slope of the orange signal. A bleed-through correction was then applied by subtracting the YFP signal divided by the bleed-through coefficient from the orange signal, resulting in a bleed-through-corrected orange signal.

Serial passage simulations

The stochastic, agent-based simulation was written in Python 3, based on earlier computational work[40], and carried out on the high performance computing cluster at University of Cambridge (CSD3). The simulation's dynamics are derived from the following infection kinetic equations[38]:

$$\frac{dV_i}{dt} = -\alpha_i(B_t + I_t)V_{i,t} + \alpha_i\beta_i B_{t-\tau}V_{i,t-\tau} - \delta_i V_{i,t}$$

$$\frac{dB}{dt} = -\sum_i \alpha_i B_t V_{i,t} + \mu B_t\left(1 - \frac{B_t}{C}\right)$$

$$\frac{dI}{dt} = \sum_i \alpha_i B_t V_{i,t} - \sum_i \alpha_i B_{t-\tau}V_{i,t-\tau}$$

In which B is the concentration of uninfected bacteria, I the concentration of infected bacteria, V_i the concentration of free phage of type i, C the bacterial carrying capacity, X_t quantity X evaluated at time t, α_i the adsorption rate of phage i, β_i the burst size of phage i, τ_i lysis time of phage i, and δ_i the free virion decay rate of phage i.

The simulation is initialised with 2 pools of 100 phage each and 10,000 susceptible cells, in a simulated well mixed volume of 10^{-5} ml. Each bacterium is a Python object and maintains two internal clocks, one representing its own cycle of growth and division, and the other representing a count down to lysis. All bacteria begin the simulation in the 'uninfected' state, at random points in their cell cycle, with their 'lysis clock' stopped.

In each simulation time-step, 'bacterial growth', 'adsorption', 'infection', 'lysis', and 'decay' substeps occur. First, in the growth step, uninfected bacteria reduce their remaining time-to-fission by one increment of time, Δt. If time-to-fission falls below zero, a new bacterium is added to the simulation and both bacteria reset their division clocks, drawing their doubling time from a normal distribution with mean $1/\mu$.

Next, in the adsorption step, a number of infecting phage of each type, ΔV_i is drawn from a Poisson distribution with mean corresponding to the expected value $\alpha_i(B_t + I_t)V_{i,t}\Delta t$ in a well-mixed population. The infecting phage are removed from the pool of free phage, and ΔV bacteria, whether infected or uninfected, are chosen randomly, uniformly and with replacement to which the phage adsorb. Each bacterium tracks how many phages of each type have adsorbed to it.

In the infection step, any bacterium which is still 'uninfected', but has at least one phage adsorbed to it changes state to 'infected (wild type)' or 'infected (mutant)' according to the nature of the adsorbed phages. In the case that a cell is infected by phages of both types, it chooses randomly in proportion to the number of adsorbed phages of each type. When a cell becomes infected it sets its internal countdown-to-lysis to a time drawn from a normal (or skew-normal) distribution with mean τ. The standard deviation and skew of this distribution depend on the phage strain. The wild type strain had a fixed standard deviation and zero skew throughout all simulations, mutant 1 varied the standard deviation across simulations and had zero skew, and mutant 2 had the same standard deviation as wild type but varied in skew across simulations. Table 8 lists all parameters used.

In the lysis step, infected cells reduce their time-to-lysis by the time increment Δt. If time-to-lysis falls below zero, the cell is deleted from the simulation, and a number of phage (wild type or mutant, according to which type of infection the cell had suffered) are released, drawn from a normal distribution with mean β.

Finally, in the decay step, each phage strain loses a number of free phage drawn from a Poisson distribution with mean $V_i\delta_i\Delta t$.

Once the number of cells has dropped below 1% of its starting value, a 'bottleneck' is carried out, simulating the transference of a small quantity of the culture to a fresh bacterial stock. The bottleneck is implemented by a 1000-fold dilution, with each phage and cell in the simulation having a 99.9% chance to be deleted, followed by adding 10,000 new susceptible cells and the stochastic process above repeats. The whole procedure is repeated until, immediately following a bottleneck, one phage pool outnumbers the other 70:30, at which point it is declared the winner and the simulation stops. If neither phage is declared the winner after 600 min of simulated time, the simulation ends in a tie.

The simulation is carried out using the same parameter values for the wild type phage in every instance, and a range of values for the mutant. Values used are presented in Table 8. For each set of values, 25 independent runs are performed and the results are tallied to arrive at a fixation rate for the mutant phage, as the proportion of runs in which the mutant won.

Table 8: Serial passage simulation parameters

Simulation parameters	
Maximum time	600 min
Volume	10^{-5} ml
Bacteria parameters	
Initial number	10,000, corresponding to a cell density of 10^{9} ml^{-1}
Carrying capacity	100,000, corresponding to a cell density of 10^{10} ml^{-1}
Doubling time	Drawn from a normal distribution with mean 20 min, standard deviation 2.5 min. Positive definite.
Steric limit	Maximum number of phages that can adsorb to a single bacterial cell: 100.
Phage parameters	
Initial number	100 wild type, 100 mutant
Adsorption rate	3×10^{-9} ml min^{-1}
Burst size	Drawn from a normal distribution with mean 150, standard deviation 50. Positive semidefinite.
Lysis time (wild type)	Drawn from a normal distribution with mean 17, standard deviation 2.5. Positive definite.
Lysis time (mutant 1)	Drawn from a normal distribution with mean 17, standard deviation varied from 2.0 to 3.0. Positive definite.
Lysis time (mutant 2)	Drawn from a skew-normal distribution with mean 17, standard deviation 2.5, skew varied from -0.88 to +0.88. Positive definite.
Decay rate	0.00013 min^{-1}

References

1. Campbell, A. The future of bacteriophage biology. *Nat. Rev. Genet.* **4**, 471–477 (2003).

2. Koskella, B., Hernandez, C. A. & Wheatley, R. M. Understanding the Impacts of Bacteriophage Viruses: From Laboratory Evolution to Natural Ecosystems. *Annu. Rev. Virol.* **9**, 57–78 (2022).
3. Schwartz, M. The adsorption of coliphage lambda to its host: Effect of variations in the surface density of receptor and in phage-receptor affinity. *J. Mol. Biol.* **103**, 521–536 (1976).
4. Weigel, C. & Seitz, H. Bacteriophage replication modules. *FEMS Microbiol. Rev.* **30**, 321–381 (2006).
5. You, L., Suthers, P. F. & Yin, J. Effects of Escherichia coli Physiology on Growth of Phage T7 In Vivo and In Silico. *J. Bacteriol.* **184**, 1888–1894 (2002).
6. Davis, K. M. & Isberg, R. R. Defining heterogeneity within bacterial populations via single cell approaches. *BioEssays* **38**, 782–790 (2016).
7. Hyman, P. & Abedon, S. T. Practical Methods for Determining Phage Growth Parameters. in *Bacteriophages: Methods and Protocols, Volume 1: Isolation, Characterization, and Interactions* (eds. Clokie, M. R. J. & Kropinski, A. M.) 175–202 (Humana Press, Totowa, NJ, 2009).
8. Kobiler, O. *et al.* Quantitative kinetic analysis of the bacteriophage λ genetic network. *Proc. Natl. Acad. Sci.* **102**, 4470–4475 (2005).
9. Wolfram-Schauerte, M., Pozhydaieva, N., Viering, M., Glatter, T. & Höfer, K. Integrated Omics Reveal Time-Resolved Insights into T4 Phage Infection of E. coli on Proteome and Transcriptome Levels. *Viruses* **14**, 2502 (2022).
10. Conners, R. *et al.* Cryo-electron microscopy of the f1 filamentous phage reveals insights into viral infection and assembly. *Nat. Commun.* **14**, 2724 (2023).
11. Wang, C., Tu, J., Liu, J. & Molineux, I. J. Structural dynamics of bacteriophage P22 infection initiation revealed by cryo-electron tomography. *Nat. Microbiol.* **4**, 1049–1056 (2019).
12. Bakshi, S. *et al.* Tracking bacterial lineages in complex and dynamic environments with applications for growth control and persistence. *Nat. Microbiol.* **6**, 783–791 (2021).

13. Jack, B. R., Boutz, D. R., Paff, M. L., Smith, B. L. & Wilke, C. O. Transcript degradation and codon usage regulate gene expression in a lytic phage. *Virus Evol.* **5**, vez055 (2019).

14. Balleza, E., Kim, J. M. & Cluzel, P. Systematic characterization of maturation time of fluorescent proteins in living cells. *Nat. Methods* **15**, 47–51 (2018).

15. Studier, F. W. The genetics and physiology of bacteriophage T7. *Virology* **39**, 562–574 (1969).

16. Van Valen, D. *et al.* A Single-Molecule Hershey-Chase Experiment. *Curr. Biol.* **22**, 1339–1343 (2012).

17. Bakshi, S. *et al.* Nonperturbative Imaging of Nucleoid Morphology in Live Bacterial Cells during an Antimicrobial Peptide Attack. *Appl. Environ. Microbiol.* **80**, 4977–4986 (2014).

18. Norman, T. M., Lord, N. D., Paulsson, J. & Losick, R. Memory and modularity in cell-fate decision making. *Nature* **503**, 481–486 (2013).

19. Wang, P. *et al.* Robust growth of Escherichia coli. *Curr. Biol. CB* **20**, 1099–1103 (2010).

20. Hardo, G., Noka, M. & Bakshi, S. Synthetic Micrographs of Bacteria (SyMBac) allows accurate segmentation of bacterial cells using deep neural networks. *BMC Biol.* **20**, 263 (2022).

21. Chen, W. *et al.* Structural changes in bacteriophage T7 upon receptor-induced genome ejection. *Proc. Natl. Acad. Sci.* **118**, e2102003118 (2021).

22. Swanson, N. A. *et al.* Cryo-EM structure of the periplasmic tunnel of T7 DNA-ejectosome at 2.7 Å resolution. *Mol. Cell* **81**, 3145-3159.e7 (2021).

23. Pao, C.-C. & Speyer, J. F. Order of Injection of T7 Bacteriophage DNA. *J. Virol.* **11**, 1024–1026 (1973).

24. Molineux, I. J. No syringes please, ejection of phage T7 DNA from the virion is enzyme driven. *Mol. Microbiol.* **40**, 1–8 (2001).

25. García, L. R. & Molineux, I. J. Rate of translocation of bacteriophage T7 DNA across

the membranes of Escherichia coli. *J. Bacteriol.* **177**, 4066–4076 (1995).

26. Kemp, P., Gupta, M. & Molineux, I. J. Bacteriophage T7 DNA ejection into cells is initiated by an enzyme-like mechanism. *Mol. Microbiol.* **53**, 1251–1265 (2004).

27. Proshkin, S., Rahmouni, A. R., Mironov, A. & Nudler, E. Cooperation between translating ribosomes and RNA polymerase in transcription elongation. *Science* **328**, 504–508 (2010).

28. Kiro, R. *et al.* Gene product 0.4 increases bacteriophage T7 competitiveness by inhibiting host cell division. *Proc. Natl. Acad. Sci.* **110**, 19549–19554 (2013).

29. Molshanski-Mor, S. *et al.* Revealing bacterial targets of growth inhibitors encoded by bacteriophage T7. *Proc. Natl. Acad. Sci. U. S. A.* **111**, 18715–18720 (2014).

30. Xu, H. *et al.* Biological Characterization and Evolution of Bacteriophage T7-△holin During the Serial Passage Process. *Front. Microbiol.* **12**, 705310 (2021).

31. Young, R. Bacteriophage lysis: mechanism and regulation. *Microbiol. Rev.* **56**, 430–481 (1992).

32. Nguyen, H. M. & Kang, C. Lysis Delay and Burst Shrinkage of Coliphage T7 by Deletion of Terminator Tφ Reversed by Deletion of Early Genes. *J. Virol.* **88**, 2107–2115 (2014).

33. Loganathan, K. & Viswanathan, B. Chapter Ten - Genome editing for phage design and uses for therapeutic applications. in *Progress in Molecular Biology and Translational Science* (ed. Singh, V.) vol. 201 203–224 (Academic Press, 2023).

34. Bull, J. J. & Wang, I. -N. Optimality models in the age of experimental evolution and genomics. *J. Evol. Biol.* **23**, 1820–1838 (2010).

35. Kerr, B., Neuhauser, C., Bohannan, B. J. M. & Dean, A. M. Local migration promotes competitive restraint in a host-pathogen 'tragedy of the commons'. *Nature* **442**, 75–78 (2006).

36. Heineman, R. H., Bull, J. J. & Hansen, T. Testing Optimality with Experimental Evolution: Lysis Time in a Bacteriophage. *Evol. Int. J. Org. Evol.* **61**, 1695–1709 (2007).

37. Kannoly, S., Singh, A. & Dennehy, J. J. An Optimal Lysis Time Maximizes

Bacteriophage Fitness in Quasi-Continuous Culture. *mBio* **13**, e03593-21 (2022).

38. Yin, J. & McCaskill, J. S. Replication of viruses in a growing plaque: a reaction-diffusion model. *Biophys. J.* **61**, 1540–1549 (1992).

39. Fort, J. & Méndez, V. Time-Delayed Spread of Viruses in Growing Plaques. *Phys. Rev. Lett.* **89**, 178101 (2002).

40. Hunter, M. & Fusco, D. Superinfection exclusion: A viral strategy with short-term benefits and long-term drawbacks. *PLOS Comput. Biol.* **18**, e1010125 (2022).

41. Hunter, M., Krishnan, N., Liu, T., Möbius, W. & Fusco, D. Virus-Host Interactions Shape Viral Dispersal Giving Rise to Distinct Classes of Traveling Waves in Spatial Expansions. *Phys. Rev. X* **11**, 021066 (2021).

42. Coshic, K., Maffeo, C., Winogradoff, D. & Aksimentiev, A. The structure and physical properties of a packaged bacteriophage particle. *Nature* **627**, 905–914 (2024).

43. Ellis, E. L. & Delbrück, M. The Growth of Bacteriophage. *J. Gen. Physiol.* **22**, 365–384 (1939).

44. Cutler, K. J. *et al.* Omnipose: a high-precision morphology-independent solution for bacterial cell segmentation. *Nat. Methods* **19**, 1438–1448 (2022).

45. Walt, S. van der *et al.* scikit-image: image processing in Python. *PeerJ* **2**, e453 (2014).

46. Steinier, Jean., Termonia, Yves. & Deltour, Jules. Smoothing and differentiation of data by simplified least square procedure. *Anal. Chem.* **44**, 1906–1909 (1972).

47. Tinevez, J.-Y. *et al.* TrackMate: An open and extensible platform for single-particle tracking. *Methods* **115**, 80–90 (2017).

48. Crocker, J. C. & Grier, D. G. Methods of Digital Video Microscopy for Colloidal Studies. *J. Colloid Interface Sci.* **179**, 298–310 (1996).

Acknowledgements

We are thankful to the members of the Bakshi Lab and Fusco lab for their support and feedback on this work.

Declarations

Funding

The research in the Bakshi lab was supported by the Wellcome Trust Award (grant number RG89305), a University Startup Award for Lectureship in Synthetic Biology (grant number NKXY ISSF3/46), an EPSRC New Investigator Award (EP/W032813/1) and a seed fund from the School of Technology at University of Cambridge. The research in the Fusco lab was supported by the Department of Physics, University of Cambridge, a Royal Society Research Grant (RGS\R2\212131) and an ERC Starting Grant/UKRI Horizon Europe Guarantee (EP/Y030141/1). Charlie Wedd was supported by the UK Engineering and Physical Sciences Research Council (EPSRC) grant EP/S023046/1 for the EPSRC Centre for Doctoral Training in Sensor Technologies for a Healthy and Sustainable Future. Georgeos Hardo was supported by United Kingdom Biotechnology and Biological Sciences (BBSRC) University of Cambridge Doctoral Training Partnership 2 (BB/M011194/1). Michael Hunter was supported by a UKRI EPSRC Doctoral Studentship from the Department of Physics, University of Cambridge (2125180). Simulations in this work were performed using resources provided by the Cambridge Service for Data Driven Discovery (CSD3) operated by the University of Cambridge Research Computing Service (www.csd3.cam.ac.uk), provided by Dell EMC and Intel using Tier-2 funding from the Engineering and Physical Sciences Research Council (capital grant EP/T022159/1), and DiRAC funding from the Science and Technology Facilities Council (www.dirac.ac.uk).

Competing interests

The authors declare no competing interests.

Authors' contributions

S.B. and D.F conceived the study and were in charge of the overall direction and planning. C.W., T.Y., A.S., M.H., D.F., and S.B. designed the experiments and simulations. C.W. carried out the microfluidics microscopy experiments, A.S. and M.H. carried out the bulk experiments, and T.Y. carried out the staining and genetic engineering of phages. C.W., R.L., G.H., and S.B designed the data analysis pipeline and carried out the data analysis. M.H., A.S., and D.F. carried out the simulations and associated analysis. C.W., D.F., and S.B., lead the manuscript writing. R.M. contributed experimental material and methods. All the other authors provided critical feedback and contributed to the manuscript.